(7) D. T. Cromer and J. T. Waber, "International Tables for X-Ray Crystallography", Vol. IV, The Kynoch Press, Birmingham, England, 1974, Table 2.2B.
(8) D. T. Cromer, ref 7, Table 2.3.1.
(9) Supplementary material.
(10) Estimated standard deviations from the mean were calculated as $[\sum(\bar{X} - X)^2/(n(n-1))]^{1/2}$.
(11) G. Alberti, U. Constantino, and J. S. Gill, *J. Inorg. Nucl. Chem.*, **38**, 1733 (1976).
(12) A. Clearfield and J. A. Stynes, *J. Inorg. Nucl. Chem.*, **26**, 117 (1964).
(13) A. Clearfield, Å. Oskarsson, and L. Kullberg, *J. Phys. Chem.*, **78**, 1150 (1974).
(14) D. Leigh and A. Dyer, *J. Inorg. Nucl. Chem.*, **34**, 369 (1972).
(15) A. Clearfield, unpublished results.

Contribution from the Departments of Chemistry, University of Virginia, Charlottesville, Virginia 22901, and University of Illinois at Chicago Circle, Chicago, Illinois 60680

Structural and Magnetic Properties of $[M(C_5H_5NO)_6]L_2$ (M = Cu, Zn; L = ClO_4^-, BF_4^-)

C. J. O'CONNOR,[1a] E. SINN,*[1a] and R. L. CARLIN*[1b]

Received June 28, 1977 AIC704633

The perchlorate and fluoborate salts of the hexakis(pyridine *N*-oxide) complexes of copper(II) and zinc(II) have been studied at 25 °C by single-crystal x-ray diffraction and EPR and in the 1–20 K region by magnetic susceptibility and heat capacity measurements. The room temperature EPR shows site splitting consistent with a static Jahn–Teller distortion while the bulk susceptibilities are isotropic ($g = 2.3$) and exhibit a large Weiss constant ($\Theta = -2.3$ K). The magnetic heat capacity is analyzed in terms of the Heisenberg linear chain model. The complexes crystallize in the space group $R\bar{3}$ with the metal atom at the center of the unit cell, which imposes a center of inversion, and a threefold rotation axis at the metal atom. In the perchlorate complexes, the anions have one Cl–O bond along the threefold axis, pointing away from the anion. The BF_4^- anions in the other complexes are positionally disordered, the predominant position being the same as in the perchlorates while a minor position has a B–F bond pointing toward the anion along the threefold axis. The cations have near-octahedral coordination about the metal atom, with metal–ligand bond lengths of 2.102 and 2.087 Å for zinc and copper, respectively. Although the Jahn–Teller effect is dynamic in the crystal lattice, space group $R\bar{3}$, the distortions from trigonal symmetry are static on the EPR time scale up to ambient temperature, the first observation of this phenomenon. Crystal data: $[Cu(C_5H_5NO)_6](ClO_4)_2$, space group $R\bar{3}$, $Z = 1$, $a = 9.620$ (2) Å, $\alpha = 81.21$ (2)°, $R = 3.6\%$ for 1076 reflections; $[Cu(C_5H_5NO)_6](BF_4)_2$, space group $R\bar{3}$, $Z = 1$, $a = 9.621$ (2) Å, $\alpha = 81.46$ (2)°, $R = 3.8\%$ for 1221 reflections; $[Zn(C_5H_5NO)_6](ClO_4)_2$, space group $R\bar{3}$, $Z = 1$, $a = 9.632$ (2) Å, $\alpha = 81.07$ (2)°, $R = 3.8\%$ for 1234 reflections; $[Zn(C_5H_5NO)_6](BF_4)_2$, space group $R\bar{3}$, $Z = 1$, $a = 9.621$ (1) Å, $\alpha = 81.25$ (4)°, $R = 3.9\%$ for 1241 reflections.

Introduction

We report the crystal structure and magnetic properties of $[M(C_5H_5NO)_6]X_2$ (where M = Cu^{2+}, Zn^{2+}; X = ClO_4^-, BF_4^-).[2] Several other members of this series of hexakis(pyridine *N*-oxide)metal(II) salts have proved to be of interest,[3] since the discovery that the crystal of the perchlorate series possesses rhombohedral symmetry.[4,5] The crystal structure of $[Ni(C_5H_5NO)_6](BF_4)_2$ shows that the fluoborate compounds, although disordered with respect to the anion, are isomorphous with the perchlorate series.[6]

Magnetic studies on the perchlorate series have revealed a consistently strong axial distortion exerted on the ion by the ligand field of the pyridine *N*-oxides. The manganese,[4] cobalt,[7] and nickel[8,9] ions all exhibit large crystal field splittings. Moreover a variety of interesting magnetic ordering phenomena have been observed in these compounds.[10-12]

The study of this series of compounds is being extended to the $S = {}^1/_2$ copper(II) ion by means of magnetic susceptibility, heat capacity, and EPR measurements. Both the perchlorate and the fluoborate compounds are shown to have very similar magnetic trigonal distortions at room temperature, although they have strikingly different magnetic properties at lower temperatures. The BF_4^- complex behaves as an $S = {}^1/_2$ planar Heisenberg antiferromagnet[13] and the ClO_4^- behaves as an $S = {}^1/_2$ linear chain Heisenberg antiferromagnet.[12]

Experimental Section

Preparations. Following previous procedures,[14] $[Cu(C_5H_5NO)_6](ClO_4)_2$ and the diamagnetic zinc host compound were prepared by mixing together stoichiometric quantities of the hydrated metal perchlorates and purified pyridine *N*-oxide in methanol. The fluoborate analogue was prepared in a similar fashion. The metal fluoborate was prepared by the addition of fluoboric acid to the metal carbonate. Single crystals of $[Zn(C_5H_5NO)_6]X_2Cu^{2+}$ (X = ClO_4^-, BF_4^-) were prepared by mixing the hydrated zinc salt with 0.1–1.0% copper salt and causing them to react with the pyridine *N*-oxide. The crystals were grown by slow evaporation of concentrated DMF solutions in a dry atmosphere.

Magnetic and Heat Capacity Data. Magnetic susceptibilities and heat capacity were measured at zero field with equipment described previously.[15] The EPR spectra were recorded on a Varian E-109 EPR spectrometer operating at X-band (9.506 GHz). The crystals were mounted in a series of orientations for rotation experiments. The axes of rotation include [100], [100] × [010], and [100] × [111]. Alignment along these axes is estimated to be within 3°.

Crystal densities were measured by flotation in chloroform/bromoform/carbon tetrachloride mixtures.

Crystal data for $[Cu(C_5H_5NO)_6](ClO_4)_2$: $CuCl_2O_{14}N_6C_{30}H_{30}$, mol wt 833, space group $R\bar{3}$, $a = 9.620$ (2) Å, $\alpha = 81.21$ (2)°, $V = 862$ Å^3, $\rho_{calcd} = 1.62$ g cm^{-3}, $\rho_{obsd} = 1.59$ g cm^{-3}, μ(Mo Kα) = 9.1 cm^{-1}; crystal dimensions (distances in mm of faces from centroid): (100) 0.115, ($\bar{1}$00) 0.115, (010) 0.085, (0$\bar{1}$0) 0.085, (001) 0.10, (00$\bar{1}$) 0.10; maximum and minimum transmission coefficients: 0.88, 0.85.

Crystal data for $[Cu(C_5H_5NO)_6]BF_4$: $CuF_8O_6N_4C_{30}B_2H_{30}$, mol wt 808, space group $R\bar{3}$, $a = 9.621$ (2) Å, $\alpha = 81.46$ (2)°, $V = 864$ Å^3, $\rho_{calcd} = 1.57$ g cm^{-3}, $\rho_{obsd} = 1.55$ g cm^{-3}, μ(Mo Kα) = 7.7 cm^{-1}; crystal dimensions (mm from centroid): (100) 0.21, ($\bar{1}$00) 0.21, (010) 0.26, (0$\bar{1}$0) 0.26, (001) 0.16, (00$\bar{1}$) 0.16; maximum and minimum transmission coefficients: 0.84, 0.81.

Crystal data for $[Zn(C_5H_5NO)_6](ClO_4)_2$: $ZnCl_2O_{14}N_6C_{30}H_{30}$, mol wt 835, space group $R\bar{3}$, $a = 9.633$ (2) Å, $\alpha = 81.07$ (2)°, $V = 864$ Å^3, $\rho_{calcd} = 1.61$ g cm^{-3}, $\rho_{obsd} = 1.57$ g cm^{-3}, μ(Mo Kα) = 9.7 cm^{-1}; crystal dimensions (mm from centroid): (100) 0.21, (100) 0.21, (010) 0.26, (010) 0.26, (001) 0.19, (001) 0.19; maximum and minimum transmission coefficients: 0.78, 0.73.

Crystal data for $[Zn(C_5H_5NO)_6](BF_4)_2$: $ZnF_8O_6N_6C_{30}B_2H_{30}$, mol wt 808, space group $R\bar{3}$, $a = 9.621$ (1) Å, $\alpha = 81.25$ (4)°, $V = 862$ Å^3, $\rho_{calcd} = 1.56$ g cm^{-3}, $\rho_{obsd} = 1.54$ g cm^{-3}, μ(Mo Kα) = 8.4 cm^{-1}; crystal dimensions (mm from centroid): (100) 0.23, (100) 0.23, (010)

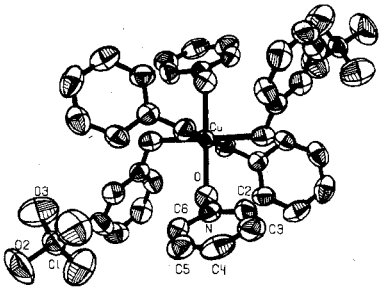

Figure 1. Stereoview of $[Cu(C_5H_5NO)_6](ClO_4)_2$.

0.16, (010) 0.16, (001) 0.10, (001) 0.10; maximum and minimum transmission coefficients: 0.83, 0.79.

For each crystal, the Enraf-Nonius program SEARCH was used to obtain 15 accurately centered reflections which were then used in the program INDEX to obtain approximate cell dimensions and an orientation matrix for data collection. Refined cell dimensions and their estimated standard deviations were obtained from least-squares refinement of 28 accurately centered reflections. The mosaicity of each crystal was examined by the ω scan technique and judged to be satisfactory.

Collection and Reduction of X-Ray Data. Diffraction data were collected at 292 K on an Enraf-Nonius four-circle CAD-4 diffractometer controlled by a PDP8/M computer, using Mo Kα radiation from a highly oriented graphite crystal monochromator. The θ–2θ scan technique was used to record the intensities for all nonequivalent reflections for which $0 < 2\theta < 50°$ for $[Cu(C_5H_5NO)_6](ClO_4)_2$ and $0 < 2\theta < 52°$ for $[Cu(C_5H_5NO)_6](BF_4)_2$, $[Zn(C_5H_5NO)_6](ClO_4)_2$, and $[Zn(C_5H_5NO)_6](BF_4)_2$. Scan widths (SW) were calculated from the formula $SW = A + B \tan\theta$, where A is estimated from the mosaicity of the crystal and B allows for the increase in width of peak due to $K\alpha_1$–$K\alpha_2$ splitting. The values of A and B were 0.60 and 0.30°, respectively. The calculated scan angle is extended at each side by 25% for background determination (BG1 and BG2). The net count is then calculated as NC = TOT − 2(BG1 + BG2), where TOT is the integrated peak intensity. Reflection data were considered insignificant if intensities registered less than 5 counts above background on a rapid prescan, such reflections being rejected automatically by the computer.

The intensities of four standard reflections, monitored for each crystal at 100 reflection intervals, showed no greater fluctuations during the data collection than those expected from Poisson statistics. The raw intensity data were corrected for Lorentz-polarization effects (including the polarization effect of the crystal monochromator) and then for absorption. After averaging the intensities of equivalent reflections, the data were reduced to 1076 independent intensities for $[Cu(C_5H_5NO)_6](ClO_4)_2$, 1221 for $[Cu(C_5H_5NO)_6](BF_4)_2$, 1234 for $[Zn(C_5H_5NO)_6](ClO_4)_2$, and 1241 for $[Zn(C_5H_5NO)_6](BF_4)_2$, of which 850, 1169, 1160, and 1039, respectively, had $F_o^2 > 3\sigma(F_o^2)$, where $\sigma(F_o^2)$ was estimated from counting statistic.[16] These data were used in the final refinement of the structural parameters.

Determination and Refinement of the Structures. $[Cu(C_5H_5NO)_6](ClO_4)_2$. The unit cell dimensions require that the metal atom be at the inversion center in each complex. Using this fact, the positions of all other nonhydrogen atoms except one ligand carbon atom were obtained from a three-dimensional Patterson synthesis. The position of the missing carbon atom was calculated.

Full-matrix least-squares refinement was based on F, and the function minimized was $\sum w(|F_o| - |F_c|)^2$. The weights w were then taken as $[2F_o/\sigma(F_o^2)]^2$, where $|F_o|$ and $|F_c|$ are the observed and calculated structure factor amplitudes. The atomic scattering factors for nonhydrogen atoms were taken from Cromer and Waber[17] and those for hydrogen from Stewart et al.[18] The effects of anomalous dispersion for all nonhydrogen atoms were included in F_c using the values of Cromer and Ibers[19] for $\Delta f'$ and $\Delta f''$. Agreement factors are defined as $R = \sum||F_o| - |F_c||/\sum|F_o|$ and $R_w = (\sum w(|F_o| - |F_c|)^2/\sum w|F_o|^2)^{1/2}$.

Anisotropic temperature factors were introduced for the nonhydrogen atoms. After refinement, the positions of the hydrogen atoms in $[Cu(C_5H_5NO)_6](ClO_4)_2$ were determined from a Fourier synthesis and these were included in the refinement. The model converged with $R = 3.6\%$ and $R_w = 4.2\%$. The parameter shifts at convergence were less than one-quarter of their estimated standard deviations. The error in an observation of unit weight is 1.8.

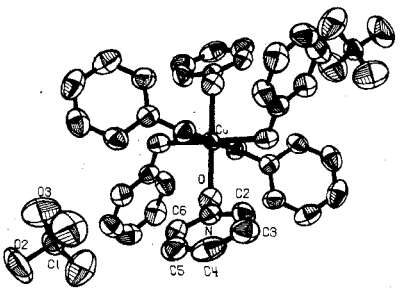

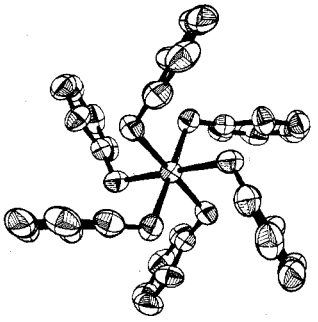

Figure 2. The $[Cu(C_5H_5NO)_6]^+$ ion in $[Cu(C_5H_5NO)_6](ClO_4)_2$ viewed down the threefold axis.

$[Cu(C_5H_5NO)_6](BF_4)_2$. Least-squares refinement was carried out using the atomic positions for the perchlorate analogue as initial parameter values. The BF_4^- anion was found to be positionally disordered, from a Fourier synthesis, in two positions, the main one (82%) corresponding to the ClO_4^- position in $[Cu(C_5H_5NO)_6](ClO_4)_2$ and the other (18%) in the opposite orientation along the threefold axis. The refinement was completed as before. The model converged with $R = 3.8\%$ and $R_w = 4.9\%$. The parameter shifts at convergence were less than one-quarter of their estimated standard deviations. The error in an observation of unit weight is 2.3. Neglect of the anion disorder raises R to 5.6%.

$[Zn(C_5H_5NO)_6](ClO_4)_2$. The calculations were carried out as above using the $[Cu(C_5H_5NO)_6](ClO_4)_2$ atomic positions as starting values. The anion showed no positional disorder. The model converged with $R = 3.8\%$ and $R_w = 5.3\%$. The parameter shifts at convergence were less than one-quarter of their estimated standard deviations. The error in an observation of unit weight is 2.0.

$[Zn(C_5H_5NO)_6](BF_4)_2$. The $[Cu(C_5H_5NO)_6](ClO_4)_2$ parameters were again used as starting values, and the refinement was carried out as before. As in the case of $[Cu(C_5H_5NO)_6](BF_4)_2$, a Fourier difference synthesis showed the BF_4^- anion to be positionally disordered, with the same two positions, with occupancies 78 and 22%, respectively. The model converged with $R = 3.9\%$, $R_w = 4.9\%$, and an error of 2.2 in an observation of unit weight. At convergence the parameter shifts were less than one-quarter of their estimated standard deviations. In each of the fluoborate complexes, the anion disorder implies two slightly different boron positions, but the improved agreement produced by inclusion of these extra parameters is not statistically significant,[20] and only a single boron position was therefore included in the final refinement for each structure. The same was observed for recalculations in the acentric space group $R3$. A final Fourier difference synthesis was featureless in each case. Tables of the observed structure factors are available.[21]

Results

Final positional and thermal parameters for $[Cu(C_5H_5NO)_6](ClO_4)_2$, $[Cu(C_5H_5NO)_6](BF_4)_2$, $[Zn(C_5H_5NO)_6](ClO_4)_2$, and $[Zn(C_5H_5NO)_6](BF_4)_2$ are given in Table I. Tables II and III contain the bond lengths and angles. The digits in parentheses in the tables are the estimated standard deviations in the least significant figures quoted and were derived from the inverse matrix in the course of least-squares refinement calculations. Figure 1 is a stereoview of $[Cu(C_5H_5NO)_6](ClO_4)_2$ showing anion and cation positions.

Table I. Positional and Thermal Parameters and Their Estimated Standard Deviations

$Cu(C_5H_5NO)_6(ClO_4)_2$

Atom	x	y	z	B_{11}	B_{22}	B_{33}	B_{12}	B_{13}	B_{23}
Cu	0.0000 (0)	0.0000 (0)	0.0000 (0)	0.0084 (1)	0.0084 (0)	0.0084 (0)	−0.0036 (2)	−0.0035 (0)	−0.0035 (0)
Cl	0.3515 (2)	0.3515 (0)	0.3515 (0)	0.0133 (2)	0.0133 (0)	0.0133 (0)	−0.0069 (3)	−0.0069 (0)	−0.0069 (0)
O	0.2165 (2)	−0.0439 (2)	0.0165 (2)	0.0139 (3)	0.0111 (2)	0.0118 (3)	−0.0043 (4)	−0.0014 (4)	0.0004 (4)
O(2)	0.4240 (7)	0.4240 (0)	0.4240 (0)	0.0307 (10)	0.0307 (0)	0.0307 (0)	−0.0242 (13)	−0.0242 (0)	−0.0242 (0)
O(3)	0.2179 (3)	0.3377 (4)	0.4322 (4)	0.0173 (4)	0.0320 (6)	0.0332 (6)	−0.0133 (8)	0.0068 (8)	−0.0014 (10)
N	0.3016 (2)	0.0466 (2)	−0.0536 (3)	0.0103 (3)	0.0100 (3)	0.0114 (3)	0.0001 (5)	−0.0018 (5)	−0.0025 (5)
C(2)	0.3347 (3)	0.0554 (4)	−0.1943 (3)	0.0125 (4)	0.0190 (5)	0.0106 (4)	−0.0083 (7)	−0.0019 (6)	−0.0057 (7)
C(3)	0.4223 (4)	0.1469 (5)	−0.2659 (4)	0.0126 (4)	0.0230 (6)	0.0132 (4)	−0.0041 (9)	0.0001 (7)	0.0002 (9)
C(4)	0.4791 (4)	0.2330 (4)	−0.1919 (5)	0.0108 (4)	0.0142 (5)	0.0247 (7)	−0.0041 (7)	0.0044 (9)	0.0005 (9)
C(5)	0.4463 (4)	0.2209 (4)	−0.0493 (4)	0.0120 (4)	0.0139 (4)	0.0232 (6)	−0.0027 (7)	−0.0027 (8)	−0.0135 (8)
C(6)	0.3570 (3)	0.1276 (3)	0.0203 (3)	0.0125 (4)	0.0123 (4)	0.0137 (4)	0.0003 (6)	−0.0023 (7)	−0.0091 (6)

Atom	x	y	z	B, Å^2	Atom	x	y	z	B, Å^2
H(2)	0.289 (3)	−0.003 (3)	−0.236 (3)	4.6 (7)	H(5)	0.479 (4)	0.275 (4)	0.010 (4)	9.5 (11)
H(3)	0.434 (4)	0.156 (4)	−0.373 (4)	8.5 (10)	H(6)	0.336 (3)	0.107 (3)	0.115 (3)	5.8 (8)
H(4)	0.538 (3)	0.294 (3)	−0.243 (3)	6.6 (9)					

$Cu(C_5H_5NO)_6(BF_4)_2$

Atom	x	y	z	B_{11}	B_{22}	B_{33}	B_{12}	B_{13}	B_{23}
Cu	0.0000 (0)	0.0000 (0)	0.0000 (0)	0.00930 (7)	0.0093 (0)	0.0093 (0)	−0.0033 (1)	−0.0033 (0)	−0.0033 (0)
F(1)	0.4199 (6)	0.4199 (0)	0.4199 (0)	0.0356 (8)	0.0356 (0)	0.0356 (0)	−0.0250 (10)	−0.0250 (0)	−0.0250 (0)
F(2)	0.2226 (3)	0.3384 (3)	0.4269 (3)	0.0189 (3)	0.0389 (5)	0.0434 (6)	−0.0169 (6)	0.0058 (6)	−0.0007 (9)
F(1′)	0.2853 (18)	0.2853 (0)	0.2853 (0)	0.0309 (22)	0.0309 (0)	0.0309 (0)	−0.0268 (27)	−0.0268 (0)	−0.0268 (0)
F(2′)	0.2710 (13)	0.3828 (10)	0.4620 (8)	0.0585 (28)	0.0323 (16)	0.0126 (8)	0.0102 (34)	0.0296 (22)	−0.0191 (17)
O	0.2168 (1)	−0.0429 (1)	0.0154 (1)	0.0151 (2)	0.0121 (2)	0.0131 (2)	−0.0042 (3)	−0.0014 (3)	0.0001 (3)
N	0.3016 (2)	0.0501 (2)	−0.0523 (2)	0.0113 (2)	0.0114 (2)	0.0121 (2)	−0.0005 (3)	−0.0016 (3)	−0.0030 (3)
C(2)	0.3312 (2)	0.0630 (3)	−0.1930 (2)	0.0133 (2)	0.0218 (3)	0.0129 (3)	−0.0081 (5)	−0.0019 (4)	−0.0051 (5)
C(3)	0.4187 (3)	0.1573 (3)	−0.2622 (3)	0.0136 (3)	0.0274 (5)	0.0147 (3)	−0.0071 (6)	0.0013 (5)	0.0042 (6)
C(4)	0.4769 (3)	0.2395 (3)	−0.1855 (4)	0.0116 (3)	0.0160 (3)	0.0297 (5)	−0.0049 (5)	0.0059 (6)	0.0012 (7)
C(5)	0.4465 (2)	0.2237 (2)	−0.0431 (3)	0.0125 (3)	0.0153 (3)	0.0264 (4)	−0.0024 (5)	−0.0009 (5)	−0.0149 (5)
C(6)	0.3580 (2)	0.1276 (2)	0.0239 (2)	0.0132 (3)	0.0143 (3)	0.0154 (3)	0.0006 (4)	−0.0021 (4)	−0.0090 (4)
B	0.3526 (7)	0.3526 (0)	0.3526 (0)	0.0158 (7)	0.0158 (0)	0.0158 (0)	−0.008 (1)	−0.0080 (0)	−0.0080 (0)

Atom	x	y	z	B, Å^2	Atom	x	y	z	B, Å^2
H(2)	0.286 (2)	0.015 (2)	−0.238 (2)	5.8 (6)	H(5)	0.491 (2)	0.269 (2)	0.022 (2)	7.1 (6)
H(3)	0.429 (2)	0.168 (3)	−0.349 (2)	6.3 (6)	H(6)	0.338 (3)	0.100 (3)	0.123 (3)	8.5 (7)
H(4)	0.534 (2)	0.293 (3)	−0.227 (2)	7.6 (7)					

$Zn(C_5H_5NO)_6(ClO_4)_2$

Atom	x	y	z	B_{11}	B_{22}	B_{33}	B_{12}	B_{13}	B_{23}
Zn	0.0000 (0)	0.0000 (0)	0.0000 (0)	0.00756 (6)	0.0076 (0)	0.0076 (0)	−0.0023 (1)	−0.0023 (0)	−0.0023 (0)
Cl	0.3514 (1)	0.3514 (0)	0.3514 (0)	0.0118 (1)	0.0118 (0)	0.0118 (0)	−0.0053 (2)	−0.0053 (0)	−0.0053 (0)
O	0.2184 (1)	0.0146 (1)	−0.0439 (1)	0.0077 (1)	0.0104 (2)	0.0100 (2)	−0.0032 (2)	−0.0034 (2)	0.0006 (3)
O(2)	0.4237 (6)	0.4237 (0)	0.4237 (0)	0.0267 (7)	0.0267 (0)	0.0267 (0)	−0.0180 (10)	−0.0180 (0)	−0.0180 (0)
O(3)	0.2166 (3)	0.4312 (3)	0.3360 (3)	0.0161 (3)	0.0303 (5)	0.0299 (5)	0.0067 (6)	−0.0143 (6)	−0.0002 (8)
N	0.3039 (2)	−0.0541 (2)	0.0476 (2)	0.0063 (2)	0.0094 (2)	0.0090 (2)	−0.0021 (3)	−0.0001 (3)	−0.0011 (3)
C(2)	0.3360 (2)	−0.1956 (2)	0.0573 (3)	0.0091 (2)	0.0101 (2)	0.0163 (3)	−0.0018 (4)	−0.0049 (4)	−0.0040 (4)
C(3)	0.4257 (3)	−0.2664 (3)	0.1501 (4)	0.0104 (3)	0.0114 (3)	0.0203 (4)	0.0018 (5)	−0.0036 (5)	0.0028 (6)
C(4)	0.4827 (3)	−0.1922 (3)	0.2343 (3)	0.0094 (2)	0.0215 (4)	0.0122 (3)	0.0050 (6)	−0.0032 (4)	0.0025 (6)
C(5)	0.4490 (2)	−0.0477 (3)	0.2210 (3)	0.0089 (2)	0.0207 (4)	0.0111 (2)	−0.0001 (5)	−0.0032 (4)	−0.0106 (4)
C(6)	0.3592 (2)	0.0203 (2)	0.1269 (2)	0.0077 (2)	0.0116 (2)	0.0112 (2)	−0.0015 (4)	−0.0011 (4)	−0.0066 (4)

Atom	x	y	z	B, Å^2	Atom	x	y	z	B, Å^2
H(2)	0.284 (3)	−0.237 (3)	0.009 (3)	5.5 (6)	H(5)	0.490 (3)	0.013 (3)	0.264 (3)	4.7 (6)
H(3)	0.444 (3)	−0.357 (3)	0.153 (3)	5.8 (7)	H(6)	0.335 (3)	0.106 (3)	0.111 (3)	5.2 (6)
H(4)	0.546 (3)	−0.231 (3)	0.301 (3)	6.0 (7)					

$Zn(C_5H_5NO)_6(BF_4)_2$

Atom	x	y	z	B_{11}	B_{22}	B_{33}	B_{12}	B_{13}	B_{23}
Zn	0.0000 (0)	0.0000 (0)	0.0000 (0)	0.00907 (9)	0.0091 (0)	0.0091 (0)	−0.0035 (2)	−0.0035 (0)	−0.0035 (0)
F(1)	0.4201 (7)	0.4201 (0)	0.4201 (0)	0.0.318 (10)	0.0318 (0)	0.0318 (0)	−0.0220 (13)	−0.0220 (0)	−0.022 (0)
F(2)	0.2229 (3)	0.3373 (4)	0.4274 (4)	0.0178 (4)	0.0407 (7)	0.0402 (8)	−0.0207 (8)	0.0045 (9)	0.000 (1)
F(1′)	0.2872 (21)	0.2872 (0)	0.2872 (0)	0.0356 (28)	0.0356 (0)	0.0356 (0)	−0.0310 (34)	−0.0310 (0)	−0.031 (0)
F(2′)	0.7264 (15)	0.6268 (13)	0.5340 (10)	0.0656 (35)	0.0413 (22)	0.0137 (10)	0.0243 (42)	0.0305 (27)	−0.023 (2)
O	0.2188 (2)	−0.0424 (2)	0.0135 (2)	0.0093 (2)	0.0116 (2)	0.0126 (2)	−0.0050 (3)	−0.0042 (3)	0.0001 (3)
N	0.3029 (2)	0.0511 (2)	−0.0526 (2)	0.0073 (2)	0.0109 (2)	0.0117 (2)	−0.0013 (4)	−0.0030 (4)	−0.0025 (4)
C(2)	0.3330 (3)	0.0651 (3)	−0.1947 (3)	0.0107 (3)	0.0205 (4)	0.0117 (3)	−0.0070 (6)	−0.0022 (5)	−0.0043 (6)
C(3)	0.4208 (3)	0.1602 (4)	−0.2621 (4)	0.0124 (4)	0.0257 (6)	0.0143 (4)	−0.0063 (8)	0.0015 (7)	0.0052 (8)
C(4)	0.4801 (3)	0.2406 (3)	−0.1857 (4)	0.0105 (3)	0.0142 (4)	0.0270 (6)	−0.0053 (6)	0.0045 (8)	0.0019 (8)
C(5)	0.4483 (3)	0.2228 (3)	−0.0420 (4)	0.0106 (3)	0.0135 (3)	0.0251 (5)	−0.0045 (5)	−0.0006 (6)	−0.0137 (6)
C(6)	0.3602 (3)	0.1270 (3)	0.0241 (3)	0.0091 (3)	0.0126 (3)	0.0145 (3)	−0.0016 (5)	−0.0020 (5)	−0.0082 (5)
B	0.3516 (9)	0.3516 (0)	0.3516 (0)	0.0157 (9)	0.0157 (0)	0.0157 (0)	−0.008 (1)	−0.0082 (0)	−0.0082 (0)

Table I (*Continued*)

Atom	x	y	z	B, Å²	Atom	x	y	z	B, Å²
H(2)	0.279 (2)	0.014 (3)	−0.242 (3)	3.7 (5)	H(5)	0.486 (3)	0.272 (3)	0.027 (3)	8.1 (9)
H(3)	0.437 (3)	0.164 (3)	−0.349 (3)	6.1 (7)	H(6)	0.335 (4)	0.114 (4)	0.115 (4)	4.8 (10)
H(4)	0.546 (3)	0.305 (3)	−0.224 (3)	6.8 (8)					

[a] The form of the anisotropic thermal parameter is $\exp[-(B_{11}h^2 + B_{22}k^2 + B_{33}l^2 + B_{12}hk + B_{13}hl + B_{23}kl)]$.

Table II. Bond Lengths (Å) and Selected Interionic Distances (Å) for $[Cu(C_5H_5NO)_6](ClO_4)_2$ (A), $[Cu(C_5H_5NO)_6](BF_4)_2$ (B), $[Zn(C_5H_5NO)_6](ClO_4)_2$ (C), and $[Zn(C_5H_5NO)_6](BF_4)_2$ (D)

Bond Lengths

	A	B	C	D
M-O	2.086 (2)	2.088 (1)	2.102 (1)	2.102 (1)
O-N	1.324 (2)	1.333 (1)	1.330 (1)	1.326 (2)
N-C(2)	1.335 (3)	1.332 (2)	1.342 (2)	1.343 (3)
N-C(6)	1.345 (3)	1.338 (2)	1.340 (2)	1.339 (3)
C(2)-C(3)	1.350 (4)	1.362 (2)	1.370 (2)	1.364 (4)
C(3)-C(4)	1.389 (4)	1.383 (3)	1.383 (2)	1.378 (4)
C(4)-C(5)	1.351 (4)	1.348 (3)	1.370 (2)	1.360 (4)
C(5)-C(6)	1.366 (4)	1.374 (2)	1.371 (2)	1.367 (3)
X-Y(1)	1.380 (6)	1.277 (4)	1.380 (4)	1.304 (4)
X-Y(2)	1.409 (6)	1.360 (4)	1.419 (4)	1.353 (4)
X-Y(1′)		1.278 (6)		1.225 (6)
X-Y(2′)		1.259 (6)		1.260 (6)
C(2)-H(2)	0.94 (3)	0.87 (2)	0.91 (2)	0.97 (3)
C(3)-H(3)	1.01 (3)	0.82 (2)	0.86 (2)	0.82 (3)
C(4)-H(4)	0.91 (3)	0.83 (2)	0.95 (2)	0.95 (3)
C(5)-H(5)	0.94 (3)	0.99 (2)	0.94 (2)	1.01 (4)
C(6)-H(6)	0.90 (3)	0.95 (2)	0.82 (2)	0.87 (4)

Selected Interionic Distances

	A	B	C	D
O-C(5)	3.461	3.469	3.452	3.432[a]
O(2)(F1)-O(2)(F1)	2.895	3.041	2.916	3.045[a]
O(3)(F3)-C(5)	3.494	3.395	3.439[c]	3.399[b]
F(1′)-C(6)		3.067		3.094[d]
F(2′)-C(4)		3.296		3.287[e]
N-C(5)	3.395	3.420	3.368	3.394[a]

[a] $1-x,-y,-z$. [b] z,x,y. [c] y,z,x. [d] x,y,z. [e] $-z,1-x,1-y$.

Table III. Bond Angles (deg) for $Cu(C_5H_5NO)_6(ClO_4)_2$ (A), $Cu(C_5H_5NO)_6(BF_4)_2$ (B), $Zn(C_5H_5NO)_6(ClO_4)_2$ (C), and $Zn(C_5H_5NO)_6(BF_4)_2$ (D)

	A	B	C	D
O-M-O ($R3$)[a]	90.23 (6)	90.37 (4)	90.47 (3)	90.44 (5)
O-M-O ($R\bar{3}$)	89.77 (6)	89.63 (4)	89.53 (3)	89.56 (5)
M-O-N	118.7 (1)	118.75 (8)	119.25 (6)	119.2 (1)
O-N-C(2)	120.9 (2)	120.7 (1)	120.0 (2)	119.8 (2)
O-N-C(6)	118.6 (2)	118.7 (1)	119.0 (1)	119.2 (2)
C(2)-N-C(6)	120.4 (2)	121.0 (1)	121.0 (1)	121.0 (2)
N-C(2)-C(3)	121.1 (2)	120.3 (2)	120.1 (2)	119.6 (2)
C(2)-C(3)-C(4)	119.4 (3)	119.6 (2)	120.0 (2)	120.6 (3)
C(3)-C(4)-C(5)	118.6 (3)	119.1 (2)	118.5 (2)	118.3 (3)
C(4)-C(5)-C(6)	120.7 (3)	120.1 (2)	120.2 (2)	120.5 (3)
N-C(6)-C(5)	119.8 (3)	119.9 (2)	120.3 (2)	120.1 (2)
X(1)-Y-X(2)	108 (1)	109 (1)	108 (1)	108 (1)
X(2)-Y-X(2) ($R3$)	111 (1)	110 (1)	110 (1)	111 (1)
X(1′)-Y-X(2′)		107 (2)		107 (1)
X(2′)-Y-X(2′) ($R3$)		112 (2)		112 (2)

[a] $R3$ and $R\bar{3}$ indicate atoms related by threefold rotation on the same side and on the other side of the inversion center, respectively.

Figure 2 shows the arrangement of the ligands around the metal atom in the $[Cu(C_5H_5NO)_6]^{2+}$ ion of $[Cu(C_5H_5NO)_6](ClO_4)_2$. The cations in the other complexes have the same arrangement of metal and ligand atoms and very similar geometries.

$[Cu(C_5H_5NO)_6](ClO_4)_2$. The ClO_4^- anion lies on the threefold axis with one Cl–O bond pointing away from the cation. The metal–ligand distance is 2.086 (2) Å and the O–Cu–O angle subtended at the copper atom by adjacent ligand oxygens on the same side of the inversion center is 90.23 (6)°.

$[Cu(C_5H_5NO)_6](BF_4)_2$. In this compound the BF_4^- ion is positionally disordered with two positions, the main one (82%) with a B–F bond on the threefold axis pointing away from the cation and the other (18%) being the reverse of this with the B–F bond on the threefold axis pointing toward the cation. The structure otherwise closely resembles that of $[Cu(C_5H_5NO)_6](ClO_4)_2$. The metal–ligand distance is 2.088 (1) Å, not significantly different from that in the perchlorate analogue. The O–Cu–O angle for oxygen atoms related by the threefold axis on the same side of the inversion center is 90.37 (4)°, marginally larger than in the perchlorate. As expected from the crystallographic symmetry, no static Jahn–Teller distortion can be observed in either of the copper structures.

$[Zn(C_5H_5NO)_6](ClO_4)_2$. The geometry of the anion and cation is quite similar to that of $[Cu(C_5H_5NO)_6](ClO_4)_2$. The metal–ligand bond (2.102 (1) Å) and the O–Zn–O angle (90.47 (3)°) for oxygen atoms related by the threefold axis are both slightly greater than in the copper complexes.

$[Zn(C_5H_5NO)_6](BF_4)_2$. Like the copper analogue this complex contains positionally disordered BF_4^- groups. The cation geometry is not significantly different from that of $[Zn(C_5H_5NO)_6](ClO_4)_2$.

The copper and zinc structures show the expected differences except, of course, for the Jahn–Teller distortion conspicuously unobserved in the copper complexes. There are small differences in the arrangements of the ionic positions in the perchlorate and fluoborate complexes. These differences are mainly associated with the BF_4^- anion disorder, which provides contacts in the fluoborate complexes that cannot be present in the perchlorates. In the copper complexes, the extra contacts provide exchange paths unique to $[Cu(C_5H_5NO)_6](BF_4)_2$ and may therefore explain the difference in the low-temperature magnetism of the two complexes.

The magnetic susceptibility of the perchlorate may be adequately described by the use of the Curie–Weiss law

$$\chi = \frac{Ng_i^2\mu_B^2 S(S+1)}{3k(T-\Theta_i)} \qquad i = \parallel, \perp \tag{1}$$

The inverse susceptibility data are plotted in Figure 3, the line being the best least-squares fit of the data to eq 1. The fitted parameters are shown in Table IV. The data require a negative Θ as shown by the intercept of the fitted line with the temperature axis. Although Θ is unexpectedly large for this compound, there is not a significant deviation from Curie–Weiss behavior down to 2 K, though there is substantial scatter in the data.

Heat capacity measurements of a 2.0-g single crystal were recorded in the temperature range 1–12 K. The only feature of the data is that, on the low-temperature side, the heat capacity of the sample begins to increase with decreasing temperature (Figure 4). The lattice heat capacity is found to be quite well described by $C_{lattice} = aF(\Theta/T)$, where the constant a is a weighting term and F is the three-dimensional Debye function. For $T < 5$ K, the asymptotic behavior is $C_{lattice}$

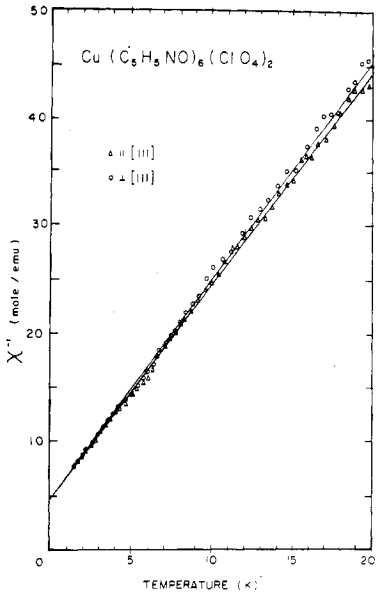

Figure 3. Curie–Weiss plots of inverse magnetic susceptibility of $[Cu(C_5H_5NO)_6](ClO_4)_2$.

Table IV. Magnetic Parameters

	$[Cu(C_5H_5NO)_6](ClO_4)_2$	$[Cu(C_5H_5NO)_6](BF_4)_2$
	Paramagnetic Resonance	
g_z	2.367 ± 0.005	2.384 ± 0.005
g_x	2.183 ± 0.005	2.202 ± 0.005
g_y	2.080 ± 0.005	2.094 ± 0.005
$A_{Cu^{63}}$	103 ± 2 Oe	104 ± 2 Oe
$A_{Cu^{65}}$	110 ± 2 Oe	110 ± 2 Oe
B_x	32 ± 5 Oe	35 ± 5 Oe
B_y	9 ± 5 Oe	18 ± 5 Oe
	Susceptibility	
$g_\parallel$	2.32 ± 0.05	
$g_\perp$	2.29 ± 0.05	
$\Theta_\parallel$	−2.36 ± 0.05 K	
$\Theta_\perp$	−2.29 ± 0.05 K	
	Specific Heat	
a	17.3 ± 0.5	
Θ_D	119 ± 1 K	
b	1.56 ± 0.05 (cal K)/mol	
J/k	−1.18 ± 0.05 K	

$= \alpha T^3$ with $\alpha = 2.2 \times 10^{-3}$ K^{-3}, which may be compared to the value of 2.5×10^{-3} K^{-3} found recently for the isomorphous Ni^{2+} compound.[9] This is to be expected because the atomic weights of nickel and copper are almost the same and the two crystal structures are isomorphous.

The magnetic contribution was first fit to a paramagnetic b/T^2 term. This fitting procedure yielded an accurate fit in the region of the minimum of the heat capacity but the calculated values rose above the data on the low side yielding unsatisfactory results. The Bonner and Fisher[22] antiferromagnetic Heisenberg linear chain model was then applied to the data and the resulting fit was of higher quality than the b/T^2 fit. Both fits of the data are shown in Figure 4 with the smooth line representing the Bonner and Fisher calculation and the dashed line representing the paramagnetic calculation. The data rise above the linear chain curve at temperatures around 1 K, but this could be due to increased magnetic exchange interaction. This agrees with the results obtained at the Kamerlingh Onnes Laboratorium, Leiden.[12] Studies done there indicate that the compound has substantial one-dimensional antiferromagnetic interactions and the onset of long range order below 1 K.

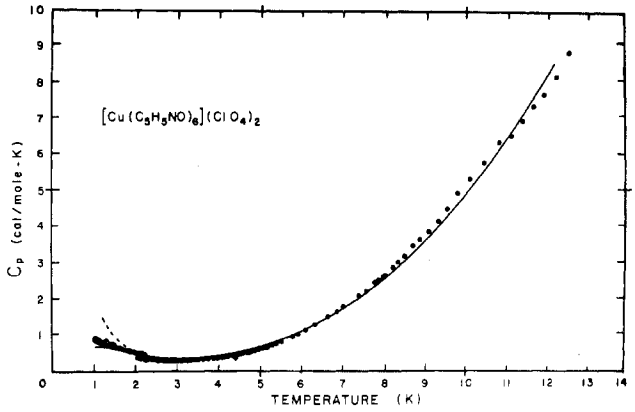

Figure 4. Plot of the heat capacity as a function of temperature for $[Cu(C_5H_5NO)_6](ClO_4)_2$.

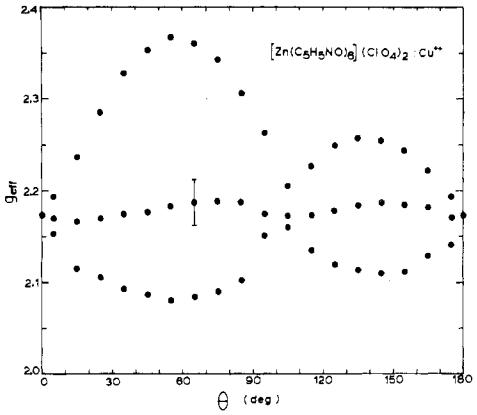

Figure 5. Angular dependence of the effective g value of $[Zn(C_5H_5NO)_6](ClO_4)_2Cu^{2+}$. The plane of rotation contains [100] and [111]. θ is angle from [100].

The EPR spectrum of the copper(II) ion may be analyzed in terms of a simple spin Hamiltonian including only the Zeeman term and a nuclear term

$$H = \mu_B \mathbf{H}\cdot\mathbf{g}\cdot\mathbf{S} + \mathbf{S}\cdot\mathbf{A}\cdot\mathbf{I}$$

where the **g** and **A** tensors are diagonalized with the magnetic field along the x, y, and z molecular axes. The hyperfine coupling constants for the x and y directions can only be approximated because the lines collapse into a single envelope. The **g** tensor as explained below has rhombic symmetry. The values of the resonnance parameters are listed in Table IV.

The spectra of $[Zn(C_5H_5NO)_6]X_2Cu^{2+}$ ($X^- = ClO_4^-, BF_4^-$) were recorded as a function of angle in the planes (100), (110), and the plane containing [100] and [111], and at three concentrations, 1.0, 0.5, and 0.1%. No significant change in the nature of the spectrum along [100] was observed when the copper impurity concentration was changed. A plot of the effective g value of the center of resonance of each set of lines vs. the angle from [111] is shown in Figure 5. It is shown that there are three lines which converge along [111] and reach a maximum near [100]. More than a few degrees away from [100], the spectrum becomes quite complicated and therefore large error bars must be associated to the effective g values. At intermediate angles, there also appear to be more than three sets of lines, probably due to exchange interactions and quadrupolar splitting. The three sets of lines plotted in Figure 5 are therefore the set with the sharpest resonances. However, the general trend of the resonance positions is apparent. Along the [111] direction (Figure 6) four broad peaks can be observed corresponding to the nuclear spin of the two copper nuclei. However, the three distinct sites can still be observed

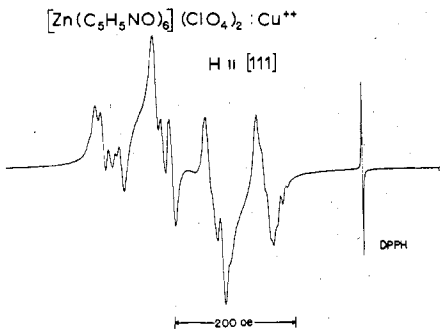

Figure 6. Spectrum of $[Zn(C_5H_5NO)_6](ClO_4)_2Cu^{2+}$ along the [111] axis.

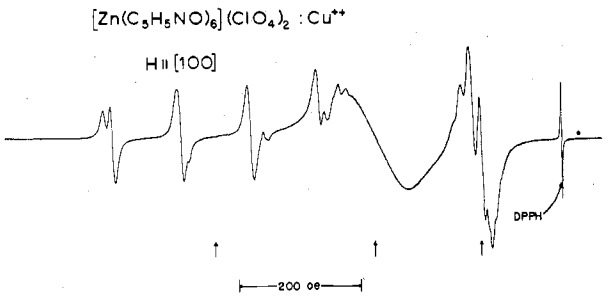

Figure 7. Spectrum of $[Zn(C_5H_5NO)_6](ClO_4)_2Cu^{2+}$ along the [100] axis.

as shoulders, due to a slight misorientation of the crystal. Near the [100] direction (Figure 7) these three sites become fully resolved.

In order to correctly assign the positions of resonance of the three sites, a theoretical splitting pattern for the lines was formulated which agreed with both the rhombic symmetry of the molecule and the rhombohedral symmetry of the lattice. If one assumes that each of the three resonances is formed by the elongation of the bonds along the x, y, and z axes, then by using the direction cosines of the field with respect to the x, y, and z axes plus a cyclic permutation of the axes will give the effective g values of three resonance sites. For the plane illustrated in Figure 5, the direction cosines can be obtained by solving three simultaneous equations. First, the equation of the plane of rotation of the crystal transferred to the molecular coordinates. This equation is given by $AX + BY + CZ = 0$, where A, B, and C are 0.9442, −0.1558, and −0.7884, respectively. This equation assumes all O–Cu–O bond angles are 90° and hence has a small intrinsic error. The coefficients to the equation were obtained from calculations based on x-ray data. It was assumed that the plane passed through the origin and that the [111] crystallographic axis was coincident with the 111 molecular axis. The other equations were $X + Y + Z = 3^{1/2} \cos\theta$, the angle from [111], and $X^2 + Y^2 + Z^2 = 1$, the normalization equation of directional cosines.

The solution of this equation gives two similar solutions corresponding to the direction of tilt of the z axis from the [100] axis. A plot of the computer-calculated effective g values is shown in Figure 8 using g_x, g_y, and g_z from the observed g values along [100]. g_{eff} was calculated from $g_{eff} = \sum_i \alpha_i^2 g_i$, where α_i are the directional cosines and i = x, y, z, plus a cyclic permutation of the g values corresponding to a transition between different geometrical Jahn–Teller distortions. There are no variables to be fit in this equation; all parameters are assigned. The calculated values show some large deviation from the observed values, possibly due to misorientation of the crystal; however, the general trend is apparent, and the two plots show a striking similarity which lends further credence to our assignment of the resonance positions in the spectra.

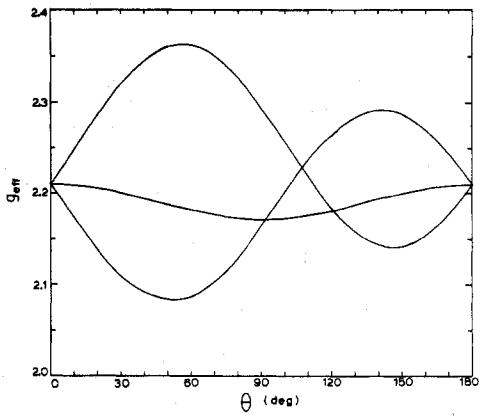

Figure 8. Calculated effective g values as a function of angle for the plane containing [100] and [111] using g values from Table IV.

A more extensive examination of the EPR spectra of these systems, including the temperature dependence, is being carried out at Nijmegen by Professor J. S. Wood.[23]

Discussion

It has been previously shown that the zinc lattice exerts a trigonal field on the impurity site.[4] The close similarity of the coordination sphere of the zinc and copper complexes is illustrated by the bond distances and angles calculated from the structure data. The copper ions which are in a purely trigonal field show nontrigonal symmetry. The explanation for this phenomen can be seen as a Jahn–Teller distortion of the symmetry of the ion to rhombic symmetry. It is quite unusual that the effect is observable at room temperature. The usual course of events is that at ambient temperatures the symmetry of the copper ion reflects the symmetry of the host, and only at lower temperatures are the various Jahn–Teller distortions frozen out due to a high energy barrier and thermal depopulation of the excited vibrational states. Many systems have been studied which show this phenomenon.[24]

It is most interesting to note that although the copper ion is distorted to rhombic site symmetry at room temperature, it still crystallizes into a rhombohedral crystal packing lattice. This leads one to believe that the distortion is dynamic on longer time scales. The time scale of the resonance experiment is of the order of 10^{-10} s, while that of the x-ray experiment is 10^2 s for the collection of one reflection and 10^5 s for the collection of an entire data set. In the time scale of the EPR experiment (10^{-10} s), the Jahn–Teller effect is static, while in the time scale of the x-ray experiment it is dynamic.

One would expect the effect of the static Jahn–Teller distortions will be observable in experiments of shorter time scales. In preliminary experiments on the far-infrared spectra (140–700 cm^{-1}), the lower symmetry of the copper complexes causes the spectrum to show two extra metal–ligand absorptions relative to the Zn^{2+}, Co^{2+}, and Ni^{2+} analogues.[25] The time scale of the experiment (10^{-13} s) is faster than the EPR experiment; therefore these results are as expected. The dynamic to static transitions previously observed in the EPR of trigonal copper ions should be observable in a slower time frame. Experiments are currently planned to examine the temperature dependence of the NMR of the copper complexes (10^{-7} s) for this effect.

Another similar copper(II) system that has a crystal structure in violation of the Jahn–Teller theorem is $K_2PbCu(NO_2)_6$ and related compounds.[26] These compounds have been under considerable recent debate[27] as the exact nature of the interactions. There appear to be three distinct crystal phases with transitions at 273 and 281 K,[28] the higher temperature associated with a dynamic to static EPR transition. The x-ray and EPR work, however, has been inves-

tigated only for the pure compound and not for dilute crystals. In the case of $K_2PbCu(NO_2)_6$, the dynamic to static transition is a long range cooperative one with the transition in the EPR caused by a crystallographic phase transition.

Although we have not yet observed a dynamic to static phase transition in the crystal structure of the copper(II) pyridine *N*-oxide species, plans are under way to examine the low-temperature crystal structure to determine if such a phenomenon will occur.

It is of interest to note that the *g* values measured from the susceptibility differ from those measured by EPR. The former is of course a macroscopic measurement, providing only the principal values of the crystal susceptibility tensor, while the latter measurements provide the microscopic or molecular values. There is therefore no inconsistency.

The major interest in the magnetic exchange interactions lies in the lower-dimensional behavior of the copper salts. Unfortunately, these phenomena are observed only below 1 K.[3,12,13] Nevertheless, the value of the exchange constant obtained here, with a very limited data set in the low-temperature region, is remarkably close to the value (-1.02 ± 0.02 K) obtained from the analysis of the data obtained below 1 K.

Registry No. $[Cu(C_5H_5NO)_6](ClO_4)_2$, 14245-15-9; $[Cu(C_5H_5NO)_6](BF_4)_2$, 23013-68-5; $[Zn(C_5H_5NO)_6](ClO_4)_2$, 23195-17-7; $[Zn(C_5H_5NO)_6](BF_4)_2$, 23013-69-6.

Supplementary Material Available: Listings of structure factor amplitudes (25 pages). Ordering information is given on any current masthead page.

References and Notes

(1) (a) University of Virginia. University of Illinois at Chicago Circle.
(2) Presented in part at the 55th Meeting of the Virginia Academy of Sciences, Petersburg, Va., 1977.
(3) C. J. O'Connor, Ph.D. Thesis, University of Illinois at Chicago Circle, 1976.
(4) C. J. O'Connor and R. L. Carlin, *Inorg. Chem.*, **14**, 291 (1975).
(5) T. J. Bergendahl and J. S. Wood, *Inorg. Chem.*, **14**, 338 (1975).
(6) A. D. van Ingen Schenau, G. C. Verschoor, and C. Romers, *Acta Crystallogr., Sect. B*, **30**, 1686 (1974).
(7) R. L. Carlin, C. J. O'Connor, and S. N. Bhatia, *J. Am. Chem. Soc.*, **98**, 685 (1976).
(8) R. L. Carlin, C. J. O'Connor, and S. N. Bhatia, *J. Am. Chem. Soc.*, **98**, 3523 (1976).
(9) J. J. Smit, L. J. de Jongh, D. De Klerk, R. L. Carlin, and C. J. O'Connor, *Physica B (Amsterdam)*, **86–88**, 1147 (1977); R. L. Carlin, C. J. O'Connor, J. J. Smit, and L. J. de Jongh, submitted for publication.
(10) H. A. Algra, L. J. deJongh, W. J. Huiskamp, and R. L. Carlin, *Physica B (Amsterdam)*, **83**, 71 (1976).
(11) K. M. Diederix, H. A. Algra, J. P. Groen, T. O. Klaassen, N. J. Poulis, and R. L. Carlin, *Phys. Lett., A*, **60**, 247 (1977); H. A. Algra, J. Bartolome, K. M. Diederix, L. J. de Jongh, and R. L. Carlin, *Physica B (Amsterdam)*, **85**, 323 (1977).
(12) H. A. Algra, L. J. de Jongh, and R. L. Carlin, to be submitted for publication.
(13) R. Navarro, H. A. Algra, L. J. de Jongh, R. L. Carlin, and C. J. O'Connor, *Physica B (Amsterdam)*, **86–88**, 693 (1977).
(14) R. L. Carlin, *J. Am. Chem. Soc.*, **83**, 3773 (1961).
(15) J. N. McElearney, D. B. Losee, S. Merchant, and R. L. Carlin, *Phys. Rev., B*, **7**, 3314 (1973).
(16) P. W. R. Corfield, R. J. Doedens, and J. A. Ibers, *Inorg. Chem.*, **6**, 197 (1967).
(17) D. T. Cromer and J. T. Waber, "International Tables for X-Ray Crystallography", Vol. IV, Kynoch Press, Birmingham, England, 1974.
(18) R. F. Stewart, E. R. Davidson, and W. T. Simpson, *J. Chem. Phys.*, **42**, 3175 (1965).
(19) D. T. Cromer and J. A. Ibers, ref 17.
(20) W. C. Hamilton, *Acta Crystallogr.*, **18**, 502 (1965).
(21) Supplementary material.
(22) J. C. Bonner and M. E. Fisher, *Phys. Rev. A*, **135**, 640 (1964).
(23) J. S. Wood and C. P. Keijzers, private communication.
(24) A. Abragam and B. Bleaney, "Electron Paramagnetic Resonance of Transition Ions", Oxford University Press, London, 1970.
(25) C. J. O'Connor, E. Sinn, and J. R. Ferraro, to be submitted for publication.
(26) D. L. Cullen and E. C. Lingafelter, *Inorg. Chem.*, **10**, 1264 (1971).
(27) B. V. Harrowfield and J. R. Pilbrow, *J. Phys. C*, **6**, 755 (1973); S. Takagi, P. G. Lenhert, and M. D. Joeston, *J. Am. Chem. Soc.*, **96**, 6606 (1974); D. Mullin, G. Heger, and D. Reinen, *Solid State Commun.*, **17**, 1249 (1975); B. V. Harrowfield, *ibid.*, **19**, 983 (1976).
(28) Y. Noda, M. Mori, and Y. Yamada, *Solid State Commun.*, **19**, 1071 (1976).

Contribution from the Ames Laboratory—Department of Energy and Department of Chemistry, Iowa State University, Ames, Iowa 50011

Synthesis and Structure of Bis(tetrapropylammonium) Tri-μ-bromo-hexabromoditungstate(2–). A Novel Odd-Electron Dimeric Anion Showing Evidence of Jahn–Teller Distortion

JOSEPH L. TEMPLETON, ROBERT A. JACOBSON, and ROBERT E. McCARLEY*

Received July 27, 1977 AIC705686

Oxidative bromination of $[(C_3H_7)_4N]^+W(CO)_5Br^-$ with 1,2-dibromoethane in refluxing chlorobenzene afforded the new compound $[(C_3H_7)_4N]_2W_2Br_9$ in high yield. Material obtained after recrystallization from acetonitrile showed simple Curie-law magnetic susceptibilities over the range 77–300 K with a magnetic moment of 1.72 μ_B. The crystals were found to be monoclinic with lattice constants $a = 36.42$ (2) Å, $b = 12.067$ (8) Å, $c = 19.62$ (1) Å, and $\beta = 95.90$ (2)°; space group $C2/c$, d(calcd) = 2.26 g cm^{-3}, d(obsd) = 2.31 g cm^{-3} with eight molecules per unit cell. Using 2255 reflections with $I \geq 3\sigma_I$ the structure was refined to $R = 0.050$ and $R_w = 0.063$. The $W_2Br_9^{2-}$ anion was found to have a confacial bioctahedral structure with d(W–W) = 2.601 (2) Å consistent with the expected W–W bond order of 2.5. An interesting distortion of the anion from D_{3h} symmetry was manifested as an effective 3° rotation of each of the planes formed by the three terminal bromine atoms on each tungsten toward the same bridging bromine atom. In this manner the real symmetry of the anion is lowered to C_{2v}. Consideration of packing effects, intramolecular nonbonded interactions, and metal–metal bonding led to the conclusion that the distortion arises from electronic effects, viz., separation of the e′ metal–metal π orbitals as dictated by the Jahn–Teller theorem.

Introduction

The study of metal–metal bonded dimeric units offers the advantage of presenting the simplest case possible for understanding attractive metal–metal interactions. In particular a large bank of data relevant to confacial bioctahedral nonahalodimetalate anions has been accumulated and analyzed.[1] Since Olsson first reported $K_3W_2Cl_9$ in 1914[2] several modifications of the general synthetic route he employed have been published.[3–5] Renewed interest in the $K_3W_2Cl_9$ species accompanied a crystal structure determination which revealed a surprisingly short W–W distance of 2.41 Å[6] as illustrated by comparison with the metal atom separation of 2.66 Å in